JOURNAL OF PROPULSION AND POWER
Vol. 26, No. 4, July–August 2010

Instability Characteristics of a Gaseous-Oxygen/Methane Pentad Injector

Robert E. Byrd Jr.* and Robert A. Frederick Jr.†
University of Alabama in Huntsville, Huntsville, Alabama 35899

DOI: 10.2514/1.41434

This experimental research characterized the modes of combustion instability produced by an impinging-jet pentad injector burning in an open cylindrical chamber. The device is being explored as a laboratory analog for unsteady mixing processes in supercritical rocket injectors. The injector burned gaseous oxygen and gaseous methane at equivalence ratios from 0.5 to 2.0 and total mass flow rates from 0.33 to 4.9 grams per second. The radial position of the injector was also varied from 0 to 76% of the chamber radius. Six high-frequency pressure transducers located around the circumference and end of the chamber simultaneously recorded pressure fluctuations at each operating point. A detailed phase analysis among the transducers allowed determination of the modes of instability. Fast Fourier transforms determined the amplitude and frequency of the primary instability at each operating point. The results show that this single-element injector exhibits spontaneous first radial, first radial-first tangential, or second tangential modes at fluctuation amplitudes up to 17% of chamber pressure. Changing the radial location of the injector changed the operating points at which maximum instability occurred. The tangential instability modes occurred with only one injector element operating under the conditions described and therefore were not driven by injector-to-injector interactions.

I. Introduction

PAST publications have reported a laboratory-scale approach to characterize and improve the combustion stability characteristics of injectors used for high-pressure liquid rocket engines [1,2]. The method uses a single-element full-scale injector, gaseous propellants, and an atmospheric combustion chamber. The approach relies on several scaling assumptions. First, assuming that each injector in the full-scale engine could behave independently in terms of the propellant mixing process, the response of a single-element injector could be used to characterize the injector stability response. Second, since supercritical fluids behave like dense gases due to reduced surface tension, low-pressure gaseous propellants could be used to simulate the mixing processes. Finally, the pressure perturbations of an atmospheric chamber were reasoned to be indicative of the pressure perturbations of the injector operating in the high-pressure environment.

For these ideas to be tested, several scaling parameters were hypothesized so that assessments in the laboratory could be applied to engine operating conditions. Although exact combustion similarity is impossible to achieve, numerous scaling criteria are available to produce physical phenomena considered most crucial to the application under investigation. Geometric similarity was preserved with a full-scale injector element. Although photographic or other types of scaling could be applied, it probably proved convenient to use existing full-scale hardware in the test device [3]. Flow conditions for similarity such as volumetric flow rate, equivalence ratio, momentum ratios, and others have been suggested. Equivalence ratio matches the chemistry characteristic of the combustion. Volumetric flow rate, in conjunction with the injector's full-scale geometric dimensions, achieves equal velocity ratio, i.e., the ratio of fuel velocity to oxidizer velocity. Two methods for attaining similar volumetric flow rates while maintaining the desired equivalence ratio are as follows: 1) heating either or both the fuel and oxidizer or 2) adding an inert gas to one or both of the propellants. The chamber diameter is scaled so that the frequencies of interest in the laboratory device could be similar to those possible in the full-scale engine. By moving the injector to positions close to the chamber wall and measuring the pressure fluctuations, the amplitude, frequencies, and modes of instabilities could then be mapped in the laboratory.

Recent work has presented additional detail on the method for rocket motor applications. Sohn et al. [4] investigated split-triplet injectors. They used scaled geometric conditions and operating conditions. Their work identified some major instability regions that correlated to chamber pressure and mixture ratio. They also presented stability margins as a function of impingement angle and derived an optimum impingement angle based on these results. The work relaxes the requirement for the operational conditions to be supercritical.

Work done by Zinn et al. [5] uses a similar laboratory device, but investigates multiple injectors and uses a liquid fuel with the goal of designing smart injectors capable of suppressing combustion instabilities. These experiments burned heptane and air and had quartz tubes as chambers. There were two injector setups used, both with a double-swirl system for the air and an axial heptane stream. The first was a single element and the other could run seven injector elements. The transparent chambers allowed for optical analysis with lasers. The studies found that changing the atomization of the injectors through variations in the flows through the swirling sections could promote or suppress combustion instability.

Past work by Cavitt et al. [6,7] presented initial stability maps for pentad injectors. Three injectors, each having a different injection angle were evaluated over a broad range of gaseous oxygen and gaseous methane conditions. The study showed that significant levels of instability, up to 17% p'/p_c, occurred in the laboratory burner. The injection angle changed the characteristics of the stability maps. The stability maps were generally repeatable. This initial study showed a single-element injector produces instability. There was only one pressure transducer on the chamber, so that the modes of instability could not be conclusively determined.

The goal of this research was to repeat and expand the conditions of the Cavitt et al. [6,7] work and to determine the exact modes of instability present at the highest amplitudes of pressure instability. The work concentrates on one injector and adds two radial positions

Presented as Paper 2008-4655 at the 44th AIAA/ASME/SAE/ASEE Joint Propulsion Conference and Exhibit, Hartford, CT, 21–23 July 2008; received 6 October 2008; revision received 21 July 2009; accepted for publication 22 July 2009.

*Graduate Research Assistant, Propulsion Research Center, Johnson Research Center, Room 102. Student Member AIAA.

†Interim Director, Propulsion Research Center, Technology Hall, Room S225; Professor, Mechanical and Aerospace Engineering. Associate Fellow AIAA.

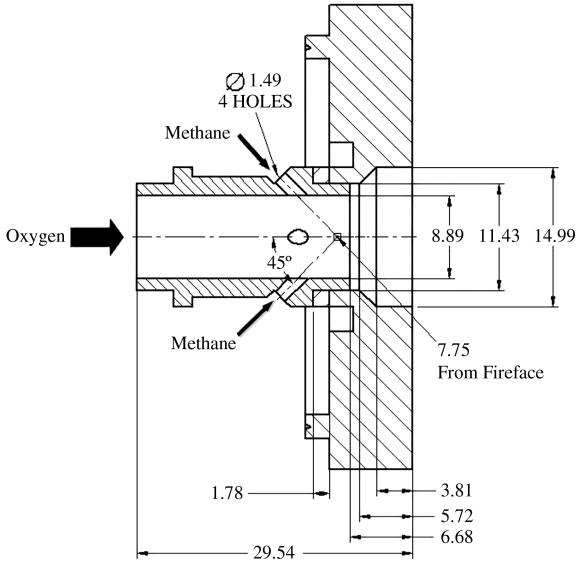

Fig. 1 Setup of 45° impinging-jet pentad injector (units in millimeters).

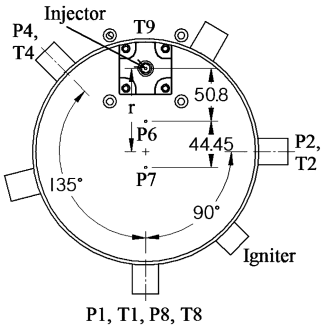

Fig. 2 Top view of resonance chamber with injector at *r* from the chamber center (units in millimeters).

of the injector in the chamber. It employs multiple high-frequency pressure transducers to determine modes of combustion instability. The major contribution, as will be presented in this article, is the verification that a single injector produces tangential instability modes.

II. Experimental Approach

A. Testing Strategy

A 45 deg impinging-jet pentad injector was evaluated at controlled propellant set points [6,7]. The impinging-jet injector is considered more unstable than coaxial types [8]. Figure 1 shows the features of the injector including a central 8.89-mm-diam oxygen passage and four evenly spaced 1.50-mm-diam fuel injection holes around the circumference. The holes were oriented at 45 deg from the central axis of the injector. Downstream of the injection holes, the injection channel expands to a 14.99 mm final diameter. The injector is not a typical pentad configuration. In traditional impinging-jet injectors, the fuel impingement point intersects downstream of the entrance to the combustion chamber. This design is typical of Russian medium-thrust hypergolic engines, in which the propellants mix in the injector post.

Three injector locations within the chamber were studied and are presented as a nondimensional radial distance. In each case, r is the radial distance from the center of the chamber, and r_c is the radius of the chamber. One location had the injector centered within the chamber ($r/r_c = 0$). Another case had the center of the injector placed at the baseline distance of $r/r_c = 0.398$. In the final setup, the center of the injector was at $r/r_c = 0.759$.

The test matrix consisted of nine tests, shown in Table 1. During each test the mass flow rate of methane was held constant while the mass flow rate of oxygen was varied through 13 setpoints (SPs), beginning at a rich equivalence ratio Φ of 2.0 and ending at a lean equivalence ratio of 0.5. A complete stability map includes a set of nine tests to produce a total of 117 individual propellant flow rate conditions. Table 1 also shows the ranges of volumetric flow rates of the fuel and oxidizer for each test. This map of operating conditions was based on the knowledge that simple changes like these can expose instabilities that may not be present at other conditions [9]. This map also reproduces the conditions of the previous experiments [6,7].

B. Test Facility

The resonance chamber was a stainless steel cylinder that was 254 mm tall with 3.2 mm thick, uncooled walls and an inner diameter of 211.1 mm. A gaseous hydrogen/oxygen igniter was attached to the side of the chamber 63.5 mm from its base. The injector's radial chamber positioning was determined by the placement of the chamber itself. When this radial location was changed the chamber was moved, leaving the injector and fire-face pressure transducers in place.

PCB 106B piezoelectric high-frequency pressure transducers, rated with a maximum step increase pressure of 1379 kPa, were placed at specified points around the combustion chamber and in-plane with the injector exit on the fire face. The transducers have an uncertainty of $\pm 0.8\%$ of reading, a rated rise time of 9 μs, and a resonant frequency of 60 kHz or greater. The high-frequency pressure measurement locations on the chamber were guided by the recommendations found in combustion instability documentation [10] and the transducer placement on the fire face came about from advice through personal communication and meetings. It was concluded that proper use of six transducers would provide the necessary information for mode determination while maintaining a sufficient data acquisition rate. The chamber used in previous work [6,7] had the same dimensions, but only allowed for a single high-frequency pressure measurement.

The combustion chamber with instrumentation locations is shown from the top in Fig. 2 and from a side in Fig. 3. Each instrumentation location was numbered from one through nine. The larger connection ports were designed for the high-frequency transducers, and type-K thermocouples were placed through the small holes above each of these. Transducers 1, 2, and 4 were located 25.4 mm above the fire face around the chamber; transducers 6 and 7 were on the fire face 50.8 and 95.25 mm away from the center of the injector, respectively;

Table 1 Test matrix of nominal flow conditions

Test	No. setpoints	$\dot{m}_{CH_4}$, g/s	Φ	$\dot{m}_{O_2}$, g/s	$\dot{m}_{total}$, g/s	$\dot{Q}_{CH_4}$, cm^3/s	$\dot{Q}_{O_2}$, cm^3/s	V_f/V_o
1	13	0.11	2–0.5	0.21–0.87	0.32–0.98	167	167–667	2.02–8.06
2	13	0.16	2–0.5	0.32–1.31	0.49–1.47	250	250–1000	2.02–8.06
3	13	0.22	2–0.5	0.43–1.74	0.65–1.96	333	333–1333	2.02–8.06
4	13	0.27	2–0.5	0.54–2.18	0.81–2.45	417	417–1667	2.02–8.06
5	13	0.33	2–0.5	0.65–2.62	0.98–2.94	500	500–2000	2.02–8.06
6	13	0.38	2–0.5	0.76–3.05	1.14–3.44	583	583–2333	2.02–8.06
7	13	0.44	2–0.5	0.87–3.49	1.31–3.93	667	667–2667	2.02–8.06
8	13	0.49	2–0.5	0.98–3.93	1.47–4.42	750	750–3000	2.02–8.06
9	13	0.55	2–0.5	1.09–4.36	1.63–4.91	833	833–3333	2.02–8.06

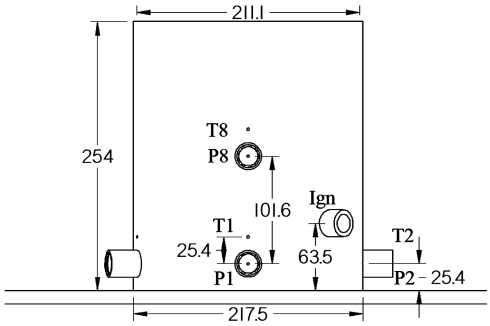

Fig. 3 Side view of resonance chamber (units in millimeters).

and transducer 8 was 127 mm above the fire face. Transducers 1, 2, 4, and 8 each had a thermocouple located 25.4 mm above them. An additional thermocouple was placed at location 9 directly across from location 1 and in plane with thermocouples 1, 2, and 4. The r represents the distance from the center of the injector to the center of the chamber. Note that the previous study, had a single pressure transducer located at the radial position P1 and at a height of 50.8 mm from the fire face. The same physical transducer was used in location 1 for both chambers to provide consistent measurements. A 30-frames/second video camera was used to view and record the appearance of the ignition event and injector flame structure from the control room.

Figure 4 provides an overview of the piping for the test stand. The bold line between the Fuel Mixer and Injector Manifold signifies an area that was modified before current testing. The previous configuration had about 150 mm of piping between these devices. This distance effectively increased to 610 mm after the modification. The length of piping upstream of the mixer stayed the same. This is shown to be potentially significant in a later discussion.

Omega mass flow controllers were used to regulate propellant flow rates to the combustion chamber. These FMA-2600A series controllers have an accuracy of $\pm 0.8\%$ of reading $+0.2\%$ full scale. They were remotely operated from the control room via of serial connection from the computer and controlled by a specifically written code in National Instruments LabVIEW 8.0 that was also used to receive and store the measured test data. In addition to the chamber measurements, there were low-frequency pressure transducers mounted upstream of the test cart, on both fuel and oxidizer lines, just upstream of the injector assembly, and on the

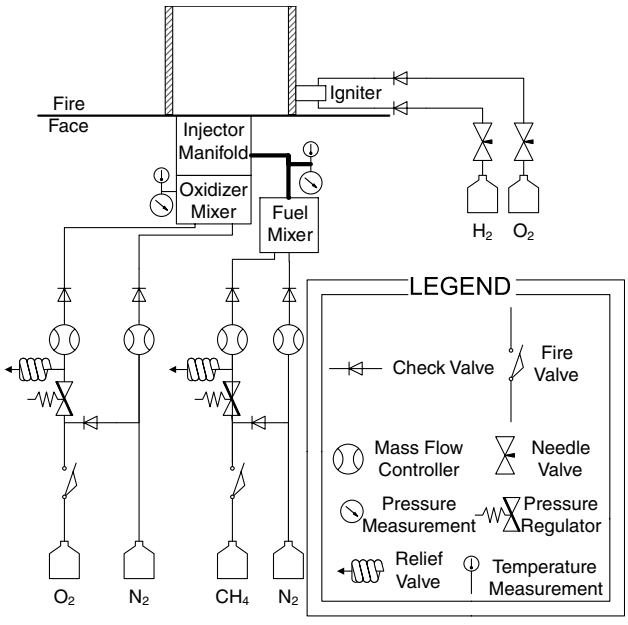

Fig. 4 Piping schematic of test stand.

igniter. Thermocouples were also placed in both lines right before the flows entered the injector assembly.

For safety reasons, the experiment was also controlled by a programmable logic controller (PLC) and a valve control board. The PLC and the control board opened and closed the valves on all the gas lines. The PLC was programmed to perform valve operations at set times automatically. The control board was also equipped with an emergency purge function to shut down the experiment.

The testing computer used two separate data acquisition (DAQ) cards and a serial port to accept data. The DAQ card used for high-frequency measurements had eight channels and a total sampling rate of 333 kHz that was split between active channels. The six transducer chamber setup was bound to a 55.5 kHz sampling rate for each transducer before the signals were passed through a low-pass filter with an 8.333 kHz cutoff frequency.

A typical test involved several steps. First, the mass flow controllers were opened to start the flow of propellants. Then the hydrogen/oxygen torch spread a flame across the face of the injector and ignited the propellants. Afterward, the propellant flow rates were changed to the conditions of the first setpoint. When the oxygen flow rate came within the tolerance of 0.075 g/s, 10,000 high-frequency pressure measurements were taken at 55.5 kHz. The next setpoint was then targeted. The nominal interval between measurements of consecutive setpoints was +35 s. Consequently, a full test generally took between 8 and 9 min. A full test matrix of nine tests, with 13 setpoints each, took nearly 2 h.

C. Instability-Mode Determination

There were two primary methods used to reach a conclusion regarding the instability mode present during combustion. The first of these compared amplitude and phase relationships among the high-frequency pressure transducers attached to the chamber. This was considered the best way to make a reliable conclusion about the mode. The second used an analytical relationship between the combustion chamber conditions and the frequency of instability for specific modes by employing the Bessel function. The latter approach was the one solely used in previous work [6,7] to make estimates of the instability mode. Ideally, the two methods should validate each other to make an even stronger case.

AI Signal Research's PC Signal software was used to perform all the necessary amplitude and phase analysis for instability-mode determination. Five key graph types were used in assessment: the fast Fourier transform (FFT) for the reference transducer (transducer 1), the FFT for the second transducer, the transfer function versus frequency between the second and reference transducers, the phase versus frequency between those transducers, and the linear coherence between the second and reference transducers. This had to be done 5 times per SP, as there were six transducers used. Transducer 1 was used as a reference for the other five transducers. The linear coherence shows how closely the two signals match each other. This value at the desired frequency must be high enough, generally greater than 0.8, to ensure reasonable comparison results.

Because the chamber was open to the atmosphere and had no converging section for pressure waves to bounce off of, the presence of significant longitudinal modes was unlikely in this application (and was verified by analysis of P1/P8 pressure data). Consequently, only transverse modes were considered in the analysis.

III. Results and Discussion

A. Stability Mapping

Significant products from testing are three-dimensional graphs that map the boundaries of instabilities and provide their peak amplitudes at the different propellant flow rate conditions [11,12]. Acting independently, these type of data can help injector design by identifying propellant flows that may present instability issues. This topic closely ties with results obtained from previous research work. Also, in order to ensure consistency between the presentation of results from more recent tests and those that were previously

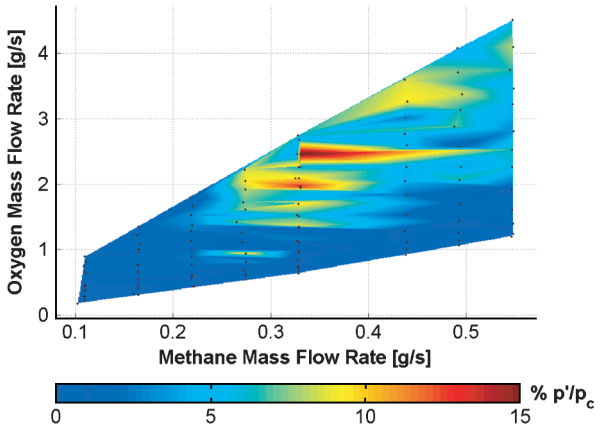

Fig. 5 Amplitude stability map for $r/r_c = 0.398$ at P1 in previous work.

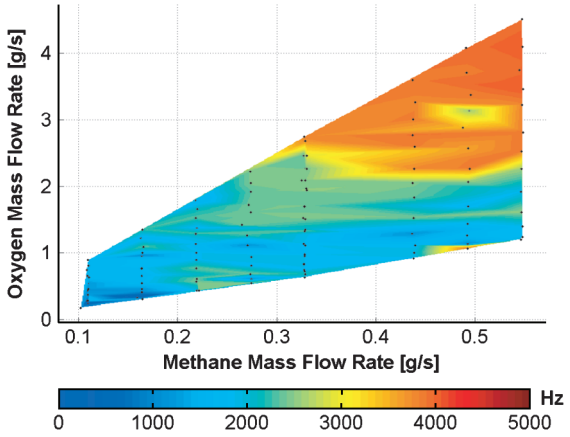

Fig. 6 Frequency stability map for $r/r_c = 0.398$ at P1 in previous work.

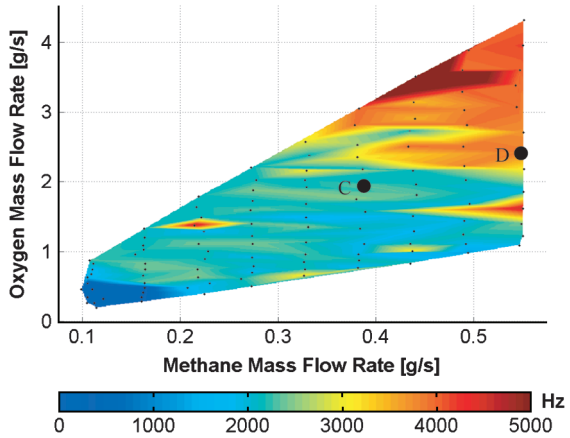

Fig. 8 Frequency stability map for $r/r_c = 0.398$ at P1

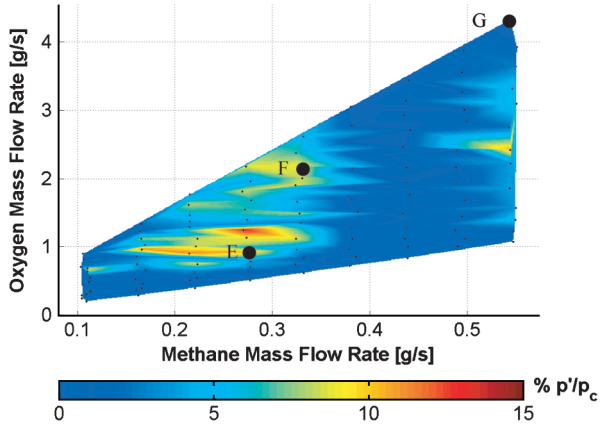

Fig. 9 Amplitude stability map for $r/r_c = 0.759$ at P1.

presented [6,7], the relevant transducer 1 data were reprocessed to obtain the figures seen in this section.

The first step in creating the stability maps was performing FFTs on the high-frequency pressure data taken from each setpoint. These FFT data were stored and used to extract the maximum peak pressure amplitude and its associated frequency at each propellant flow condition. Once this has been done, the resulting amplitudes, frequencies, and flow rates are copied and stored to be mapped. The maps are three-dimensional, but shown in two dimensions with the third axis represented by a color-coded scale. Selected results of previous testing, presented in Figs. 5 and 6, show two regions of pressure fluctuations above 10% p'/p_c as well as at least two clearly different areas in measured frequencies. The top-right area of the frequency map in Fig. 6 represents frequencies in the 4000 Hz range, while much of the other regions are closer to 2000 to 2500 Hz.

Figures 7 and 8 show the corresponding results for transducer 1 in current investigation. The frequency map shows a similar frequency trend as exists in the results from previous tests. There is a major amplitude difference compared to previous work, however. The results from later tests show much lower amplitudes in nearly all regions of the map. Possible reasons for this decrease include transducer calibration, propellant line changes, weather effects, and others. The most probable cause may be a change in the methane line plumbing upstream of the injector (refer to Fig. 4). The previous data were repeatable within that older configuration. Likewise the current configuration produces repeatable results.

The alphabetic labeling of C and D at certain spots on Figs. 7 and 8 signifies setpoints chosen for more detailed analysis. The criteria for these selections will be discussed in the following section.

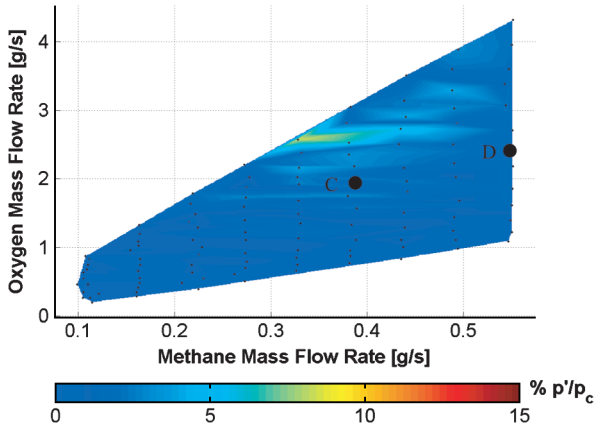

Fig. 7 Amplitude stability map for $r/r_c = 0.398$ at P1.

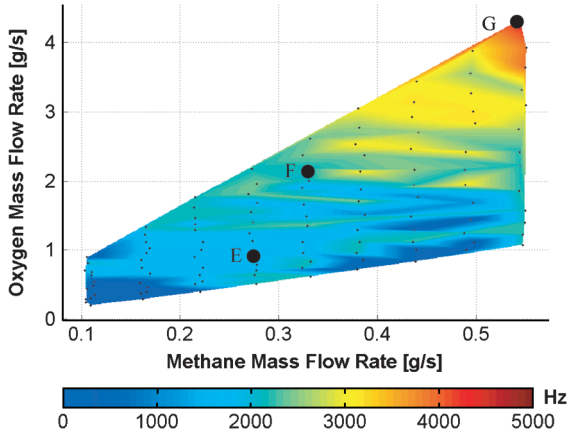

Fig. 10 Frequency stability map for $r/r_c = 0.759$ at P1.

Table 2 Summary of analyzed setpoints for all transducers

Test ID	SP	r/r_c	Φ	$\dot{m}_{CH_4}$, g/s	$\dot{m}_{O_2}$, g/s	Freq., Hz	Max p'/p_c, %	Mode
A	000-30-07	0.000	0.90	0.33	1.46	2200	13	1R
B	000-50-10	0.000	0.65	0.55	3.36	2200	17	1R
C	398-35-08	0.398	0.80	0.38	1.91	2500	13	1R
D	398-50-07	0.398	0.90	0.55	2.43	4000	8	1T1R
E	759-25-05	0.759	1.2	0.27	0.91	1700	10	2T
F	759-30-11	0.759	0.6	0.33	2.18	2200	9	1R
G	759-50-13	0.759	0.5	0.55	4.37	3200	10	1T1R

Figures 9 and 10 show the amplitudes and frequencies measured by transducer 1 at $r/r_c = 0.759$. Compared to stability maps at $r/r_c = 0.398$, these are very different. There is still an overall trend toward higher frequencies moving toward the top-right corner of the map, but the actual frequencies found are quite different. This location is much more dominated by lower frequencies. In addition, strong amplitudes show themselves in a somewhat different region than before. Like the earlier stability maps, points labeled E, F, and G are setpoints that will be looked at in more detail in the following section.

Initially, centered tests ($r/r_c = 0$) were not a part of the plan. Because of this, there were not enough tests run to complete a full stability map. It served to validate the amplitude and phase analysis method. It was widely believed that only radial modes would exist with such a configuration. Therefore, it seemed like a good place to start to ensure reasonable analysis results.

B. Instability-Mode Results and Discussion

Selected setpoints were analyzed at each of the three injector locations. Figures 7–10 provided information that aided in the selection of setpoints to further study. In general, areas that showed clear frequencies and have amplitudes near 10% p'/p_c went under preliminary analysis. The setpoints that were chosen had consistent frequencies among transducers, amplitudes near 10% p'/p_c for at least one transducer, and had a sufficiently high coherence ratings after all transducer measurements were quickly analyzed using PC Signal. The seven setpoints that were selected are labeled A through G and summarized in Table 2. Setpoints C through G can be seen on Figs. 7–10. Conditions A and B were from $r/r_c = 0$ testing, which was run at a limited number of setpoints.

1. *Injector at* $r/r_c = 0$

Conditions A and B in Table 2 are from this configuration. Test B provided some of the highest peak amplitudes seen, in particular transducer 2 (17% p'/p_c). Figure 11 displays the time-domain signals for each transducer. The FFT data for transducer 1 are given in Fig. 12. In Fig. 13, the phases of the pressure signals relative to transducer 1 are given along with a possible node line configuration.

This confirmed that this was a first radial mode. Moreover, the pressure waves in the time domain were smooth and very sinusoidal compared to those from other injector locations. The FFTs provided a clear peak as well. When considering the order of the mode, the phase relationships between transducers 1, 6, and 7 were revisited. Because transducer 6 was 180 deg out of phase with respect to the others, it was concluded that this was most likely a 1R instability mode.

2. *Injector at* $r/r_c = 0.398$ *(Baseline)*

The goal of this injector location was to determine the instability modes under the same radial injector position previously tested with

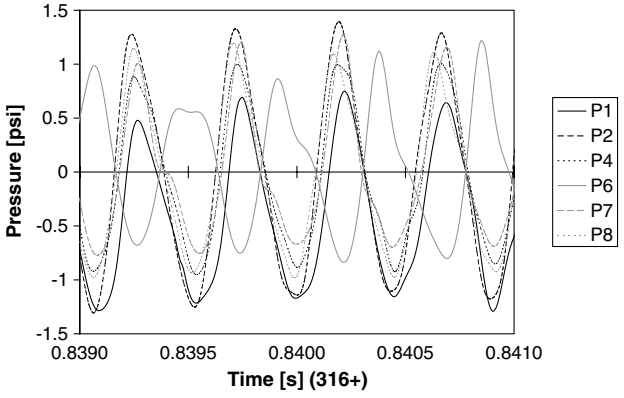

Fig. 11 Time-domain transducer data for test B.

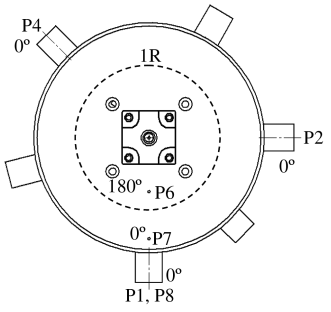

Fig. 13 Phase data for test B.

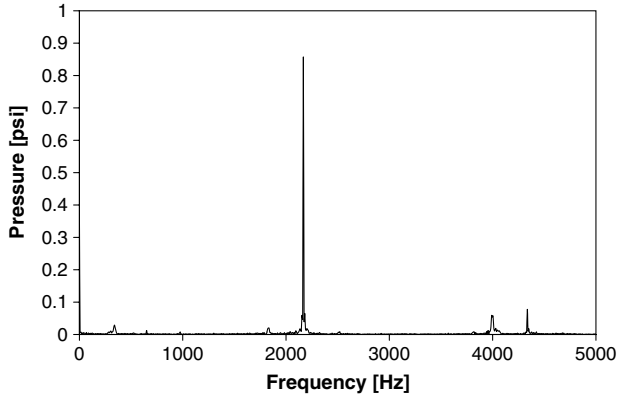

Fig. 12 FFT of transducer 1 for test B.

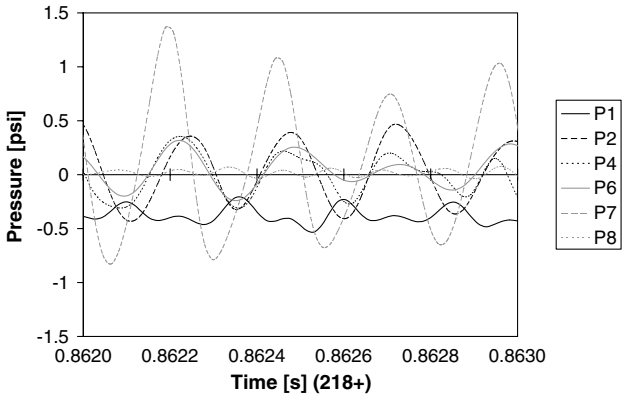

Fig. 14 Time-domain transducer data for test D.

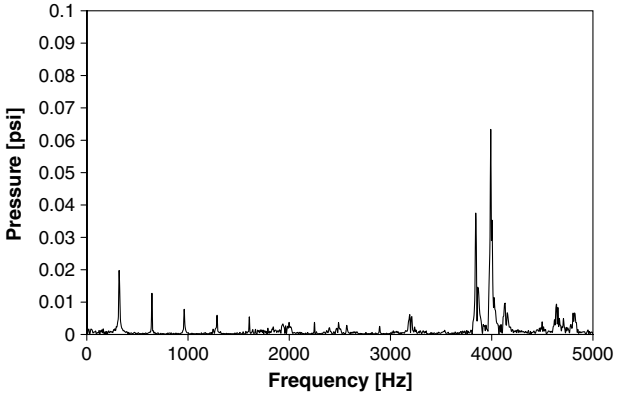

Fig. 15 FFT of transducer 1 for test D.

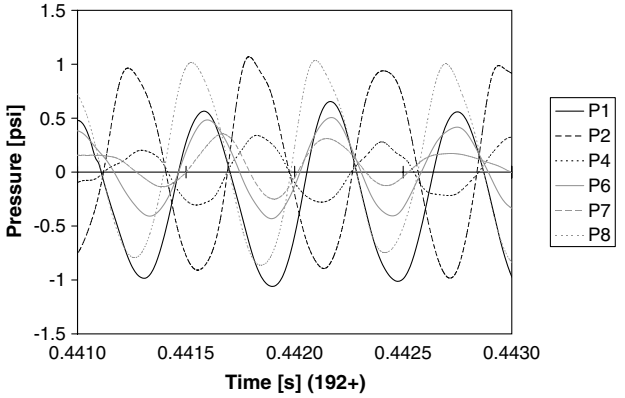

Fig. 17 Time-domain transducer data for test E.

the single transducer chamber. This allowed for comparisons to be done with earlier conclusions made with one high-frequency pressure transducer. The center of the injector is 63.5 mm from the chamber wall, closest to location 9. Conditions C and D in Table 2 show information from this location. The transducer data can be seen in Fig. 14 for test D. Figure 15 shows the FFT data for transducer 1. An illustration of the phase data from this setpoint can be seen in Fig. 16.

These data suggested that a tangential and radial combined mode was possible. Higher amplitudes near the center meant that a radial mode is present. However, the phase relationships forced a tangential mode. The order of these modes could be narrowed down by noting the physical shapes of these modes. Because of the much lower amplitude of transducer 1 to transducer 2, a 1T1R was the most reasonable. These two were physically 90 deg from each other and thus the same distance from a potential 2T node line. Therefore, their amplitudes should have been similar. However, a 2T1R mode was still possible. This configuration did not have the tangential mode resolution to make a concrete assessment from phase perspective because both P6 and P7 were located on the same side of any potential tangential node line.

This process was also conducted at a setpoint where the frequency was 2500 Hz and definitely appeared to be a radial mode. The highest amplitude was in the center and there was a seeming transition from peak to trough from transducer 6 to 7 and then toward the wall.

3. *Injector at $r/r_c = 0.759$*

The final injector location to be discussed, $r/r_c = 0.759$, provided the most exciting and controversial findings. Because tangential modes are most pronounced when the injector is close to the chamber wall, it was placed 25.4 mm from the wall. There were also some earlier concerns that testing this close to the wall may cause a burn-through on the chamber and that water-cooling would be necessary to perform such experiments. However this was not as serious of an issue as initially thought and testing proceeded without the chamber being water-cooled. It should be noted, however, that the wall near the flame did become glowing red during testing at higher methane flow rates.

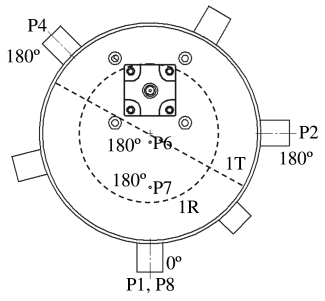

Fig. 16 Phase data for test D.

This was a very interesting injector location; consequently, much more data were taken. Setpoints E, F, and G in Table 2 pertain to this location. Test E had one of the strongest amplitudes found in testing. Figure 17 contains the transducer data for that setpoint. The FFT data for transducer 1 are given in Fig. 18. Once again, the data were analyzed in PC Signal and phase data are illustrated in Fig. 19.

The frequency found here was very interesting compared to other tests of this injector at the two previous locations. A consistent 1700 Hz peak was not observed in other tests and had an amplitude well above 10% p'/p_c, which seemed difficult to obtain with the newer chamber. The amplitudes of transducer 7 also showed that a radial mode was not likely considering its close proximity with the center and low magnitude. The phase relationships of transducers 2 and 4 required that a tangential mode be present. The order of this mode was determined by phases of transducers 6 and 7. The order had to be an even number for opposite sides of a node line to be in phase with each other. The placement of transducers, however, did not have the resolution to further pin down the tangential mode order. Nevertheless, this information did provide enough confidence to suggest that a 2T mode was active. Two other setpoints were considered resulting in the following determinations: 1R at 2200 Hz and 1T1R at 3200 Hz.

4. *Graphical Bessel Function Analysis*

These instability-mode frequencies can be seen graphically in Fig. 20. Shown are the frequencies of potential instability as a function of sound speed for the chamber dimensions, calculated using the Bessel function process. Each horizontal line is the frequency of the dominant peak of a testing setpoint. This type of information can be used in at least two specific ways to establish what mode is active. The conditions that affect the chamber acoustics can be determined so that a speed of sound can be calculated. Another approach would be to use instability-mode knowledge already obtained in order to arrive at an effective speed of sound. Because of its relative simplicity, determining the radial mode by other methods

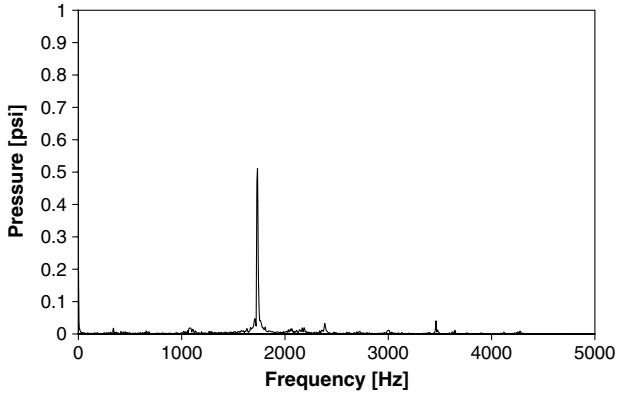

Fig. 18 FFT of transducer 1 for test E.

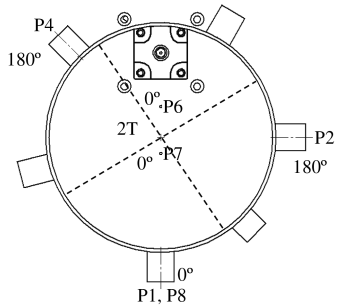

Fig. 19 Phase data for test E.

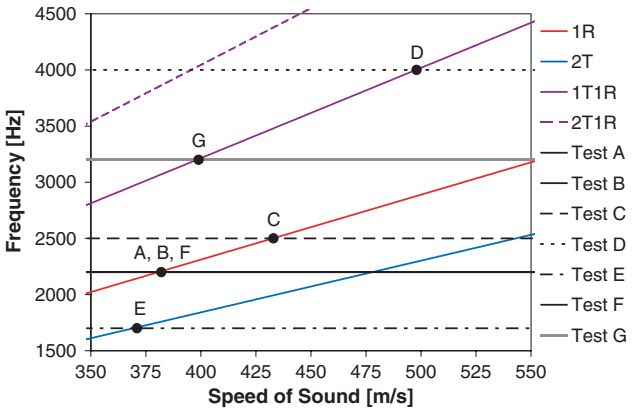

Fig. 20 Instability-mode frequencies vs speed of sound.

and using its frequency provides a good starting estimate for the speed of sound to be applied to other setpoints.

From Fig. 20 and the determinations made for tests A, B, C, and F, a 1R mode at 2500 Hz would suggest a speed of sound of about 430 m/s, and one at 2200 Hz would exist at around 380 m/s. It should be noted that all three injector locations are placed on this graph, which creates some variations between determined modes. It can be seen for tests D, E, and G that there are corresponding modes at speeds of sound within a reasonable range of these estimates. This was helpful in further study of the combined mode found in test D. A 1T1R mode is possible at about 500 m/s. Though there is a difference of about 70 m/s between this speed and that of 430 m/s radial mode, this is a relatively small change, about a 16% increase. Considering the higher mass flow rates and more stoichiometric mixture of test D, this difference seems almost expected. If this combined mode is a 2T1R mode, then the matching sound speed is about 400 m/s. This is also fairly close to that of the known 1R mode, but does not have as much physical rationale for the change. These observations provide some justification for the method of using known instability modes to estimate other modes.

IV. Conclusions

The research project validated that tangential instability modes can be produced by a single-element injector for the method investigated. Additionally, a method was successfully applied to make instability-mode determinations by comparing the relative phases and amplitudes of multiple, specifically positioned high-frequency pressure transducers and by analytical means using the Bessel function.

These methods found that in the case of the centered injector ($r/r_c = 0$), for the setpoints investigated a 2200 Hz 1R instability was present. A 1R mode existed at about 2500 Hz and a 1T1R mode occurred at about 4000 Hz when the injector was placed at $r/r_c = 0.398$. When the injector was placed at $r/r_c = 0.759$, it was concluded that a 1700 Hz 2T, a 2200 Hz 1R, and a 3200 Hz 1T1R existed. The discovery of a tangential mode with a single injector proves contrary to the notion that these modes only occur because of the interaction between multiple injector elements.

It was decided that recent changes made to the fuel piping affected the amplitudes of instability compared to previous work while maintaining similar frequencies at a given setpoint. The study does not yet prove that the scaling analogy is correct with a full-scale engine, but shows that the modes of interest are produced to enable further investigation into this analogy.

Acknowledgments

This work was sponsored by NASA Constellation University Institutes Project under grant NCC3-989 with Claudia Meyer as the Project Manager. In addition, the guidance of Jim Hulka (Jacobs ESTS Group) and Matt Casiano (NASA Marshall Space Flight Center) has been greatly appreciated. The others at the University of Alabama in Huntsville (UAHuntsville) Propulsion Research Center have been a big help as well: team members Huy Huyhn, Shawn Ikard, Jason Bush, and Dennis Creech; Facility Engineer Tony Hall; Dave Lineberry; and Visiting Scholar Vladimir Bazarov. We also posthumously express our gratitude to Clark Hawk for his leadership of the Propulsion Research Center at UAHuntsville.

References

[1] Dexter, C., Fisher, M., Hulka, J., Denisov, K., Shibanov, A., and Agarkov, A., "Scaling Techniques for Design, Development, and Test," *Liquid Rocket Thrust Chamber: Aspects of Modeling, Analysis, and Design*, Progress in Astronautics and Aeronautics, AIAA, Reston, VA, 2004, pp. 553–600.

[2] Dranovsky, M., "Model Firing Tests for Selection of Injector Head Elements," *Combustion Instabilities in Liquid Rocket Engines: Testing and Development Practices in Russia*, Progress in Astronautics and Aeronautics, Vol. 221, AIAA, Reston, VA, 2007, pp. 171–190.

[3] Hulka, J. R., "Scaling of Performance in Liquid Propellant Rocket Engine Combustion Devices," AIAA Paper 2008-5113, July 2008.

[4] Sohn, C. H., Seol, W., Shibonav, A., and Pikalov, V., "Combustion Stability Boundaries of the Subscale Rocket Chamber with Impinging Jet Injectors," *Journal of Propulsion and Power*, Vol. 23, No. 1, 2007, pp. 131–139. doi:10.2514/1.19937

[5] Zinn, B. T., Lubarsky, E., and Neumeier, Y., "Real-Time Control for Optimal Liquid Rocket Combustor Performance," U.S. Air Force Research Lab., SR-AR-TR-06-0020, Wright-Patterson AFB, OH, Dec. 2005.

[6] Cavitt, R., Frederick, R., Byrd, R., and Bazarov, V., "On the Laboratory Scale Survey of Pentad Injector Stability Characteristics," AIAA Paper 2007-5587, July 2007.

[7] Cavitt, R., Frederick, R., and Bazarov, V., "Laboratory Scale Survey of Pentad Injector Stability Characteristics," *Journal of Propulsion and Power*, Vol. 24, No. 3, 2008, pp. 534–540. doi:10.2514/1.32618

[8] Culick, F., and Yang, V., "Overview of Combustion Instabilities in Liquid-Propellant Rocket Engines," *Liquid Rocket Engine Combustion Instability*, edited by V. Yang, and W. Anderson, Vol. 169, Progress in Astronautics and Aeronautics, AIAA, Washington, D.C., 1995, pp. 3–36.

[9] Fisher, S., Dodd, F., and Jensen, R., "Scaling Techniques for Liquid Rocket Combustion Stability Testing," *Liquid Rocket Engine Combustion Instability*, edited by V. Yang and W. Anderson, Vol. 169, Progress in Astronautics and Aeronautics, AIAA, Washington, D.C., 1995, pp. 545–563.

[10] Harrje, D., and Reardon, F., "Liquid Propellant Rocket Combustion Instability," NASA SP-194, 1972.

[11] Byrd, R., "Laboratory-Scale Injector Instability Mode Assessment," M.S. Thesis, Univ. of Alabama in Huntsville, Huntsville, AL, 2008.

[12] Byrd, R., Huynh, H., and Frederick, R., "Injector Element Instability Mode Assessment in a Laboratory-Scale Burner," AIAA Paper 2008-4655, July 2008.

D. Talley
Editor-in-Chief